PHYSICAL REVIEW E **86**, 045201(R) (2012)

Finite-time statistics of scalar diffusion in Lagrangian coherent structures

Wenbo Tang* and Phillip Walker
School of Mathematical & Statistical Sciences, Arizona State University, Tempe, Arizona 85287, USA
(Received 25 July 2012; published 11 October 2012)

We study the variability of passive scalar diffusion via the statistics of stochastic particle dispersion in a chaotic flow. We find that at intermediate times when the statistics of individual trajectories start to exhibit scaling-law behaviors, scalar variance over the entire domain exhibits multimodal structure. We demarcate the domain based on Lagrangian coherent structures and find that the conditional statistics exhibit strong unimodal behavior, indicating coherence of effective diffusion among each Lagrangian partition of the flow.

DOI: 10.1103/PhysRevE.86.045201 PACS number(s): 05.45.−a, 05.40.Fb, 05.60.−k, 47.27.De

Advances in nonlinear dynamical systems methods in the past decade have enabled the objective extractions of coherent structures from chaotic flow data that has general time dependencies. These coherent structures, obtained from measures associated with the Lagrangian trajectories of fluid parcels, retain kinematic properties under arbitrary translation and rotation of the coordinate system and are thus frame independent and robust [1,2].

Highly popularized due to its efficiency, the finite-time Lyapunov exponents (FTLE) is one of the most used mathematical tools to study the variability of Lagrangian mixing [3] and to identify Lagrangian coherent structures (LCS) [1]. Roughly speaking, the FTLE field provides the different rates at which nearby trajectories separate over finite time. Topological properties of the FTLE are used to study the details of LCS [4].

While theoretical developments based on FTLE help identify barriers of Lagrangian mixing in deterministic flow fields, little has been studied in their relations with stochastic processes and diffusion. Experiments and observations suggest that transient-time diffusion follow LCS [5]. An *ad hoc* effective diffusivity was constructed based on FTLE [6]. A few recent studies explored the effects of random noise on FTLE [7,8]. In considering the LCS subject to realistic random noises in a flow model, it is found that well and poorly mixed *zones* appear [8], bounded by the most distinguished mixing barriers (Lagrangian skeletons) in deterministic studies [4].

Recent experiments [9] and theories [10] on scalar intermittency indicate that the existence of coherent structures leads to non-Gaussian statistics and anomalous diffusion. Because of the observed alignment of concentration gradients with the LCS skeletons [5], it is promising to associate passive scalar statistics with the Lagrangian topology, and pin down the effect that LCS has on diffusion.

The goal of this work is to analyze stochastic processes associated with a nonlinear, chaotic flow where coherent structures are prevalent, and obtain finite-time statistics crucial to understandings of intermittency. By partitioning the domain into different regions using FTLE, we pinpoint the role of flow topology on the statistics. We are aware of one prior study on conditional statistics in chaotic flows, which does not involve stochasticity, and used the frame dependent Lagrangian Okubo-Weiss parameter [11,12]. Addition of random noise and use of FTLE make the present work realistic and objective.

To make our discussion concrete, we adopt the following phenomenology. Coherent structures that have long-time correlations are present and slowly evolving. There is sufficient scale separation between the coherent structures and subgrid-scale uncertainties, and we impose a Gaussian white noise on the advection of scalars. For easy identification and partitioning of coherent structures, we consider the kinematic model of Bickley jet [13].

Model and parameter. The Bickley jet model arises from studies on the stability of a zonal shear flow where the zonal velocity $u \propto \operatorname{sech}^2 y$. The eigensolution of the governing equation admits two neutral waves where by superposition with the mean shear flow can generate overlap regions that exhibit chaotic trajectories. As a result, vortices, jets, and mixing zones coexist in this model. Parametric dependence of the deterministic dynamics on Bickley jet has been studied before [14,15].

The stream function of the Bickley jet is given by

$$\psi = \tanh y + \operatorname{sech}^2 y \sum_{i=1}^{2} \varepsilon_i \cos k_i (x - c_i t), \tag{1}$$

where ε_i, k_i, and c_i are the amplitude, wave number, and phase speed of the waves. Parameters are chosen to be dynamically consistent with governing equations [16]:

$$\Delta = \sqrt{1 - \frac{3}{2}\beta}, \quad \beta \in \left(0, \frac{2}{3}\right);$$
$$c_{1,2} = \frac{1}{3}(1 \pm \Delta), \quad k_{1,2}^2 = 6c_{1,2}, \tag{2}$$

hence the dynamics is given in a three-parameter family $(\beta, \varepsilon_{1,2})$. It has been found that for different choices of the parameters, the phase portrait may exhibit transition between homoclinic connections and heteroclinic connections, as well as transition between a persistent zonal jet and the breaking of this central barrier [14]. To retain clearly identifiable topological features, we choose the parameters as $\varepsilon_1 = 0.1$, $\varepsilon_2 = 0.3$, and $\beta = 0.6144$: the integrable jet coexists with chaotic zones.

It is computationally unmanageable to study the topological dependence of scalar statistics on LCS from direct numerical simulations (DNS) of the Fokker-Planck equations, while maintaining a high resolution for initial conditions. As such, we resort to the computation of a random displacement model

*wenbo.tang@asu.edu

(RDM) based on stochastic differential equations [17]. To be precise, we generate a large ensemble of realizations governed by the equations

$$\dot{x} \equiv u = -\psi_y + \sqrt{2\kappa}\dot{W}_1, \quad \dot{y} \equiv v = \psi_x + \sqrt{2\kappa}\dot{W}_2, \quad (3)$$

where ψ is given in Eq. (1), κ (=0.001 in our baseline case) is a diffusivity that controls the magnitude of the uncorrelated random walks $\dot{W}$. The RDM uses RK4 for the deterministic and explicit Euler for the stochastic terms.

We use a DNS solver [18] to resolve the evolution of the Fokker-Planck equations over time, up to when the various moments of scalar statistics start to exhibit scaling-law behavior. Nine of such runs are performed, with initial conditions evenly distributed across all regions, to determine the time of integration necessary for robust statistics. With the parameters chosen, the numerically determined time of integration $t = 1000$. In the baseline case, this corresponds to a time scale at which diffusion will take a concentrated scalar to spread over a unit area.

The RDM equation (3) is solved for the nine initial conditions to determine the number of realizations needed in any of the regions. 50 000 realizations per initial condition are chosen such that the probability density function generated by DNS and RDM match well for all cases. A sampling grid of 144×64 in the x and y directions is chosen to fit on a 14-node, 224-CPU cluster.

Finally, to speed up the computations, the integration time step for RDM is chosen as $\Delta t = 0.01$. This time stepping is insufficient for accurate deterministic trajectories because of the large integration time and sensitive dependence on initial conditions, but is sufficient as far as convergence in probability density is concerned. However, much smaller tolerance and time steps are chosen for deterministic trajectories to obtain the FTLE field.

After generating all realizations, various moments of scalar dispersion are computed based on the ensemble of displacements that originate in the same initial condition or the same LCS to study the topological dependence.

Analyses. Defining the finite-time deformation tensor of the flow as $\partial \boldsymbol{x}(\boldsymbol{x}_0,t_0;t_0+t)/\partial \boldsymbol{x}_0$, the largest eigenvalue $\lambda(\boldsymbol{x}_0,t_0;t_0+t)$ can be obtained from singular value decomposition. The FTLE is then $\sigma = \ln(\lambda)/t$ for spatially and temporally dependent λ.

We compare the flow topology and variability of scalar variances in Fig. 1. Figure 1(a) shows the deterministic forward-time FTLE field after integration time $t = 1000$ at a resolution of 576×256. By parameter selection we preserve the central barrier region, seen as the wavy structure with relatively low FTLE values around $y = 0$. On both sides of this region, we find the boundaries of the jet, which take smooth transition of FTLE values, up to highlighting FTLE ridges which separate the jet boundaries from the chaotic zones. Inside the chaotic zones, the FTLE values appear to be very random. This indeed is due to the fine structures of the heteroclinic tangles [14], which are not resolved at this resolution. Outside of the chaotic zones, we find the structures separating them from a shear-dominant exterior flow.

Figures 1(c) and 1(d) show the variances of scalar displacement in the x and y directions, respectively. The variances are computed based on the initial conditions given. For a set of realizations released at $\boldsymbol{x}_0$, $\mathrm{var}\boldsymbol{x}(\boldsymbol{x}_0,t_0;t) = \sum_{r=1}^{50\,000}[\boldsymbol{x}_r(\boldsymbol{x}_0,t_0;t) - \overline{\boldsymbol{x}_r(\boldsymbol{x}_0,t_0;t)}]^2$. The overline denotes average based on initial conditions, and the bold font $\boldsymbol{x}_r$ denotes the computation of variance separately for x and y. As seen, the contour map indicating variability of variances correspond very well with the deterministic flow topology, except for low-value patches inside the chaotic zone, indicating low dispersion. In this zone, although deterministic trajectories are chaotic, the ensemble of stochastic trajectories behave quite regular after sufficient time. At the core of the chaotic zone, the cluster of nearby ensembles separates much less than trajectories on the edge of the chaotic zone. This low

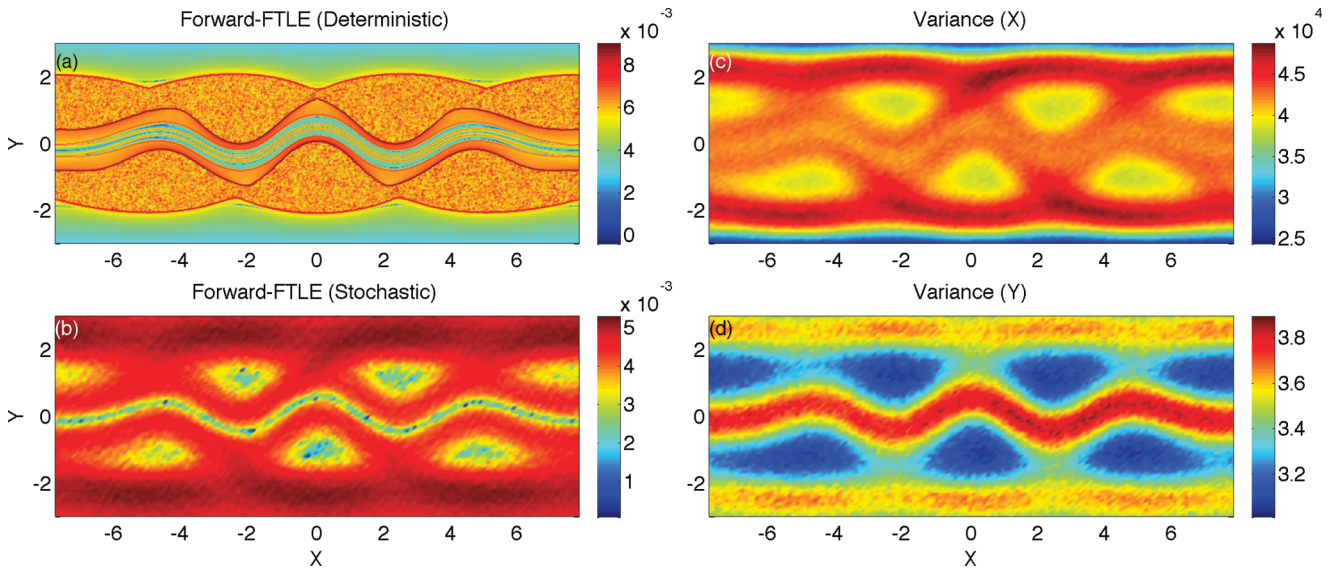

FIG. 1. (Color online) Comparison among LCS and variances, all dependent on the initial conditions and at $t = 1000$. (a) Forward-time FTLE based on deterministic trajectories. (b) Forward-time FTLE based on stochastic mean trajectories. (c) Variance of x displacements. (d) Variance of y displacements.

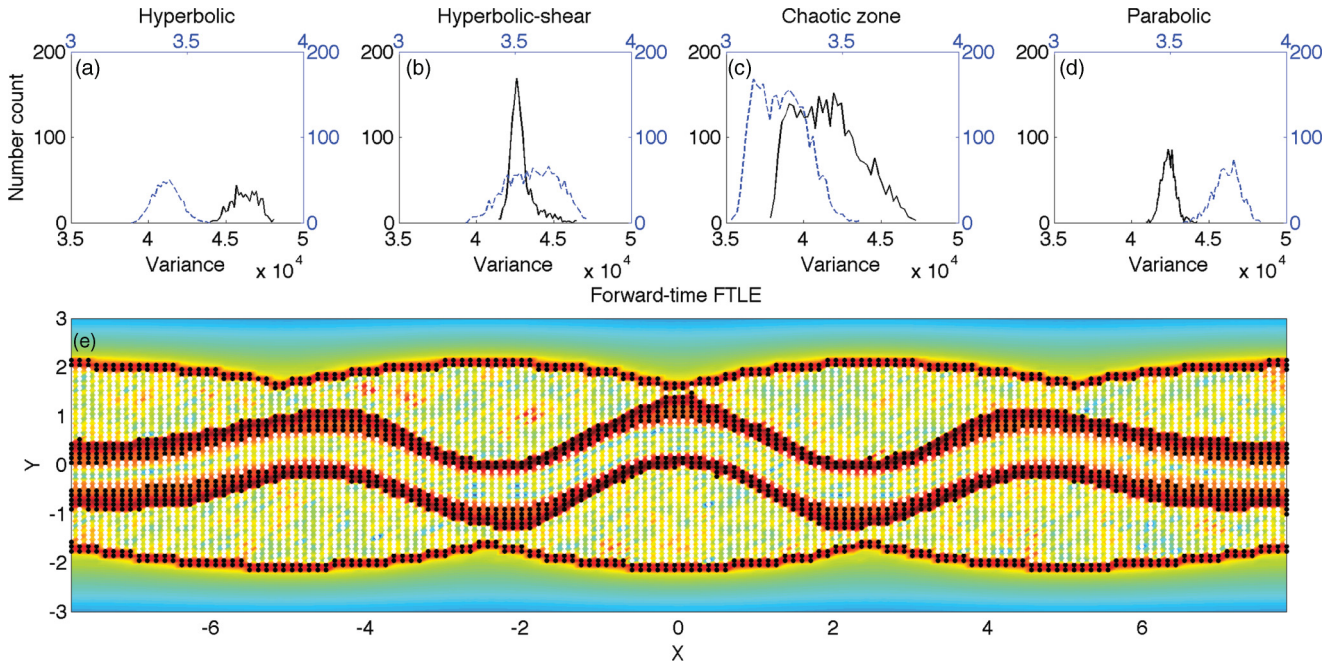

FIG. 2. (Color online) Conditional statistics of variances and FTLE in different partitions of the flow. (a) Outer barriers that are hyperbolic. (b) Inner barriers that transition from hyperbolic to parabolic structures. (c) Chaotic zone between the hyperbolic barriers. (d) Parabolic central jet region. (e) Partitioning of domain superimposed on FTLE.

separation is also seen in Fig. 1(b) on FTLE based on the mean trajectories.

A common feature of these contour maps is the almost uniform value of variances in each of the partition of LCS (except for the chaotic zone). This behavior indicates that the diffusion process is coherent within each individual coherent structure. Motivated by this observation, we show conditional statistics of the variances in Fig. 2. We partition the domain using the *deterministic* FTLE since we hope to relate diffusion processes to *a priori* knowledge of coherent structures without having to compute the stochastic differential equations. Partitioning of the domain is based on locating the contours corresponding to the largest slopes in the FTLE field and eliminating spurious results in the chaotic zone via visual inspection. Figure 2(e) shows the deterministic FTLE along with the partitions. The white points denote the partition of jet in the center and the chaotic zones on the two sides. The black points denote the two inner barriers separating the jet and the chaotic zones, and the two outer barriers separating the chaotic zones and the exterior.

The probability density function (pdf) of variances of displacements are given in the top panels of Figs. 2(a)–2(d), with Fig. 2(a) the two outer barriers that exhibit hyperbolic behavior, 2(b) the two inner barriers that mark transition between hyperbolic and parabolic regions, 2(c) the chaotic zones between the hyperbolic regions, and 2(d) the central jet. Because of the difference in the number of sampling points, the histogram in different regions encloses different areas under the curves. In these panels, the black solid (gray dashed line, blue online) curves associate with the black (gray, blue online) axes, corresponding to the variances in x (y). As expected, in all except for the chaotic zone, variances exhibit unimodal behavior with relatively narrow width, indicating high probability in a small range of diffusivity. The residence time of trajectories in the center of the chaotic zone is longer than those close to the hyperbolic barriers; a continuous transition of initial conditions from the center towards the edge of this zone gives rise to the relatively flat and wide pdf in variances as seen in Fig. 2(c).

In order to measure the effective diffusion in each of the LCS, we study conditional statistics across all realizations that start in the same zone and their temporal evolution. The pdf of relative displacement from the mean is considered. For each initial condition $\boldsymbol{x}_0$ in the same LCS, we compute the pdf of $\delta\boldsymbol{x}_r = \boldsymbol{x}_r(\boldsymbol{x}_0,t_0;t) - \overline{\boldsymbol{x}_r(\boldsymbol{x}_0,t_0;t)}$, where the overline denotes average at time t of all realizations originating from $\boldsymbol{x}_0$. As such, $\delta\boldsymbol{x}_r$ has a zero mean.

As time progresses, it is found that the pdf approaches a self-similar profile. The histograms for $\delta\boldsymbol{x}_r$ are shown in Fig. 3 for the different partitions, with proper rescaling. The hyperbolic zone in Fig. 3(a) corresponds to the combination of the two boundary regions [Figs. 2(a) and 2(b)]. The chaotic [Fig. 3(b)] and parabolic [Fig. 3(c)] zones cover the same regions as Figs. 2(c) and 2(d). The histogram over the entire domain is shown in Fig. 3(d). Again, the black (gray, blue online) curves and axes associate with the x (y) statistics. They are shifted horizontally for more clarity. The lonely solid curves in each panel correspond to $t = 100$ and those that fall onto the self-similar profile are $t = 700$ (dashed line), 800 (dotted line), 900 (dashed-dotted line), and 1000 (solid line). These four curves are almost indistinguishable in Fig. 3, with only small variabilities due to a slow relaxation to a Gaussian.

The δy statistics appear to be symmetric and relatively simple. At $t = 100$, all regions appear to be non-Gaussian with a flatter peak and slightly fatter tail. The self-similar

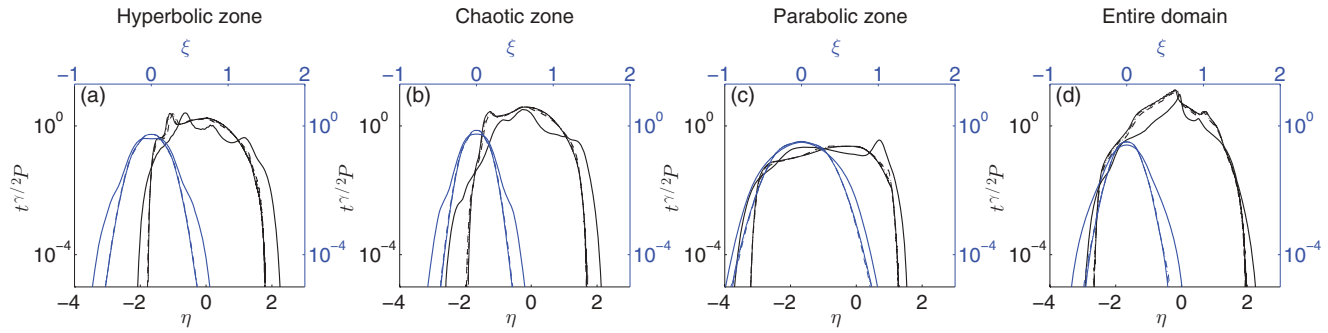

FIG. 3. (Color online) Conditional statistics on scalar dispersion in different partitions of the flow.

profile already approaches Gaussian. It takes the form of $P(\delta y,t) = t^{-\gamma/2} f(\xi), \xi = \delta y/t^{\gamma/2}$, where f is a scaling function, ξ a scaled coordinate, and γ the exponential decay rate. It is noted that $\gamma = 1$ indicates normal diffusion, $\gamma < 1$ indicates subdiffusion, and $\gamma > 1$ indicates superdiffusion. The exponent γ is found to take values of 0.75, 0.82, 0.62, and 0.66 for Figs. 3(a)–3(d), respectively. In all cases, the y dispersion is subdiffusive. The central barrier region has the least decay rate, consistent with the fact that barriers inhibit cross-jet transport.

For δx statistics, the rate of decay in the central peak and the rate of expansion in the two tails are somewhat different. The self-similar profile takes the form of $P(\delta x,t) = t^{-\alpha/2} g(\eta)$, $\eta = \delta x/t^{\beta_\pm/2}$. Here, g is a scaling function, α is the exponential decay rate, $\beta_\pm$ correspond to the expansion of tails in positive and negative branches of δx. The differential expansion rate is due to the bias in zonal transport: scalars caught in the jet displace at different speed as those in the chaotic and outer shear zones. Relatively, the parabolic jet moves in the positive x direction, the chaotic and shear zones move in the negative x direction, leading to different growth rates in the positive and negative tails. For scalars initially in hyperbolic and chaotic zones, a significant amount of realizations diffuse into the outer shear zone, leading to the peaks in pdf at negative values of η in Figs. 3(a) and 3(b). In the parabolic zone, not as many realizations get trapped in the center of the chaotic zone because of the jet boundaries serving as transport barriers, hence no similar peak can be found. In any region, the zonal pdfs are strongly non-Gaussian. The expansion rates β_+ in the positive branch are 1.75, 1.75, 1.8, 1.8; the expansion rates β_- in the negative branch are 1.9, 1.6, 1.45, 1.6 and the decay rates α are 1.75, 2, 1.4, 2 for Figs. 3(a)–3(d), respectively. Henceforth, the zonal transport is superdiffusive with the respective decay rates.

We also study the dependence of statistics based on variable diffusivity κ. Because of the linearity in the diffusion problem, such dependence varies almost linearly, when κ reduces in half the topological features of the variances at $t = 1000$ is similar to those of the original κ at $t = 500$. However, the actual value of variances varies differently among different partitions. In particular, variances in the central barrier vary as κ^{-2} because of the ballistic style trajectories. In order to reveal such dependence, we show in Fig. 4 three values of κ, from left to right, each reduced in half, $\kappa = 0.001, 0.0005, 0.00025$, and three values of t, from left to right, each increased twice, $t = 100, 200, 400$. As seen, the geometry of these structures is very similar, except that the scalar variance grows with different exponents in respective partitions. As such, one can study the κ dependencies based on Lagrangian partitions of the coherent structures and the respective growth rates within each partition. Not shown in Fig. 4, at very large κ, variance structures do not associate with FTLE topology because of the strong homogenization across all zones.

Conclusions. Finite-time statistics of scalar diffusion associate well with FTLE. A simple partition of the domain based on FTLE values already reveals the almost uniform capability of individual LCS in diffusing a scalar. This suggests the use of LCS in studying anomalous diffusion because of their

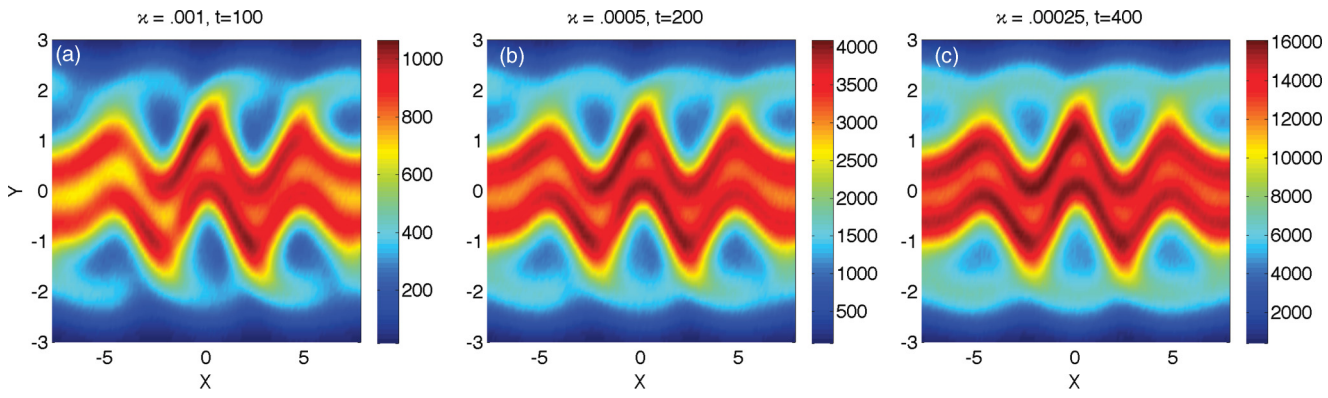

FIG. 4. (Color online) Dependence of zonal variance on diffusivity and time.

objectivity in structure classification. Our results confirm the importance of studying coherent structures in zones in addition to focusing on finding the location of the barriers. Applying the recent results of geodesic LCS theory [19] or using the probabilistic approach based on transfer operators [20] to improve the objectivity in domain partitions may bring further insights on the statistics we obtain here. Such studies will be reported elsewhere.

Acknowledgments. We acknowledge the support of Grant No. NSF-DMS-1212144. W.T. acknowledges the hospitality at the Lorentz center workshop on "Coherent structures in dynamical systems" and the 2012 GFD program at Woods Hole Oceanographic Institution, which fostered extensive discussion with D. del-Castillo-Negrete. We also thank the helpful comments from three anonymous referees which improved the quality of this paper.

[1] G. Haller, Phys. D (Amsterdam) **149**, 248 (2001); S. C. Shadden, F. Lekien, and J. E. Marsden, *ibid*. **212**, 271 (2005).

[2] G. Haller, Phys. Fluids A **13**, 3365 (2001); J. Fluid Mech. **525**, 1 (2005); T. Peacock and J. O. Dabiri, Chaos **20**, 017501 (2010); G. Haller, Phys. D (Amsterdam) **240**, 574 (2011).

[3] R. T. Pierrehumbert, Phys. Fluids A **3**, 1250 (1991); R. T. Pierrehumbert and H. Yang, J. Atmos. Sci. **50**, 2462 (1993).

[4] M. Mathur, G. Haller, T. Peacock, J. E. Ruppert-Felsot, and H. L. Swinney, Phys. Rev. Lett. **98**, 144502 (2007); W. Tang, M. Mathur, G. Haller, D. C. Hahn, and F. H. Ruggiero, J. Atmos. Sci. **67**, 2307 (2010); W. Tang, G. Haller, and P. W. Chan, J. Appl. Metero. Clim. **50**, 325 (2011).

[5] G. A. Voth, G. Haller, and J. P. Gollub, Phys. Rev. Lett. **88**, 254501 (2002); Y. Lehahn, F. d'Ovidio, M. Lévy, and E. Heifetz, J. Geophys. Res. **112**, C08005 (2007).

[6] F. d'Ovidio, E. Shuckburgh, and B. Legras, J. Atmos. Sci. **66**, 3678 (2009).

[7] A. B. Olcay, T. S. Pottebaum, and P. S. Krueger, Chaos **20**, 017506 (2010); W. Tang, J. E. Taylor, and A. Mahalov, Phys. Fluids **22**, 126601 (2010).

[8] W. Tang, B. Knutson, A. Mahalov, and R. Dimitrova, Phys. Fluids **24**, 063302 (2012).

[9] B. Castaing, G. Gunaratne, F. L. Heslot, L. Kadano, A. Libchaber, S. Thomas, X. Wu, S. Zaleski, and G. Zanetti, J. Fluid Mech. **204**, 1 (1991); J. P. Gollub, J. Clarke, M. Gharib, B. Lane, and O. N. Mesquita, Phys. Rev. Lett. **67**, 3507 (1991); T. H. Solomon, E. R. Weeks, and H. L. Swinney, *ibid*. **71**, 3975 (1993); O. Cardoso, B. Gluckmann, O. Parcollet, and P. Tabeling, Phys. Fluids **8**, 209 (1996).

[10] H. Chen, S. Chen, and R. H. Kraichnan, Phys. Rev. Lett. **63**, 2657 (1989); V. Yakhot, S. Orszag, S. Balachandar, E. Jackson, Z. She, and L. Sirovich, J. Sci. Comput. **5**, 199 (1990); A. Pumir, B. Shraiman, and E. D. Siggia, Phys. Rev. Lett. **66**, 2984 (1991); R. M. McLaughlin and A. J. Majda, Phys. Fluids **8**, 536 (1996); D. del-Castillo-Negrete, *ibid*. **10**, 576 (1998).

[11] B. Kadoch, D. del-Castillo-Negrete, W. J. T. Bos, and K. Schneider, Phys. Rev. E **83**, 036314 (2011).

[12] G. Haller and G. Yuan, Phys. D (Amsterdam) **147**, 352 (2000).

[13] W. G. Bickley, Philos. Mag. **23**, 727 (1937).

[14] D. del-Castillo-Negrete and P. J. Morrison, Phys. Fluids A **5**, 948 (1993).

[15] I. I. Rypina, F. J. Beron-Vera, M. G. Brown, H. Kocak, M. J. Olascoaga, and I. A. Udovydchenkov, J. Atmos. Sci. **64**, 3595 (2007); F. J. Beron-Vera, M. J. Olascoaga, M. G. Brown, H. Kocak, and I. I. Rypina, Chaos **20**, 017514 (2010).

[16] F. B. Lipps, J. Fluid Mech. **12**, 397 (1962).

[17] B. Oksendale, *Stochastic Differential Equations: An Introduction with Applications*, 3rd ed. (Springer, Berlin, 1992); J. P. Crimaldi, J. R. Cadwell, and J. B. Weiss, Phys. Fluids **20**, 073605 (2008); W. Tang, J. E. Taylor, and A. Mahalov, *ibid*. **22**, 126601 (2010).

[18] P. Moin and K. Mahesh, Ann. Rev. Fluid Mech. **30**, 539 (1998).

[19] G. Haller and F. J. Beron-Vera, Phys. D (Amsterdam) **241**, 1680 (2012).

[20] S. E. Scott, T. C. Redd, L. Kuznetsov, I. Mezić, and C. K. R. T. Jones, Phys. D (Amsterdam) **238**, 1668 (2009); E. M. Bollt, A. Luttman, S. Kramer, and R. Basnayake, Int. J. Bifurcation Chaos **22**, 1230012 (2012).